

APPROXIMATING MAPS INTO MANIFOLDS WITH LOWER CURVATURE BOUNDS*

SIMON JACOBSSON[†], RAF VANDEBRIL[‡], JOERI VAN DER VEKEN[§], AND NICK VANNIEUWENHOVEN[¶]

Abstract. Many interesting functions arising in applications map into Riemannian manifolds. We present an algorithm, using the manifold exponential and logarithm, for approximating such functions. Our approach extends approximation techniques for functions into linear spaces so that we can upper bound the forward error in terms of a lower bound on the manifold’s sectional curvature. Furthermore, when the sectional curvature of a manifold is nonnegative, such as for compact Lie groups, the error is guaranteed to not be worse than in the linear case. We implement the algorithm in a Julia package and apply it to two example problems from Krylov subspaces and dynamic low-rank approximation, respectively. For these examples, the maps are confirmed to be well approximated by our algorithm.

Key words. Riemannian manifold, manifold exponential, manifold logarithm, function approximation, constructive approximation.

AMS subject classifications. 15A69, 53Z99, 65D15

1. Introduction. Approximation theory is concerned with approximating functions with simpler functions. Classic approximation theory studies schemes for approximating real-valued functions. For example, univariate schemes like interpolation or regression [23, 62], but also multivariate schemes like hyperbolic crosses, sparse grids, and greedy approximation [61]. More recently, multivariate function approximation methods based on tensor decompositions have been extensively investigated [12, 13, 14, 30, 31, 32, 38, 39, 57, 58]. All of these schemes are naturally extended to approximate vector-valued functions by applying them component-wise.

Many interesting functions arising in applications have some further structure, like matrix-valued functions having *low-rank* or *orthogonal* values. For instance, the present work was conceived to address difficulties encountered in the context of reduced order models of a microstructure materials engineering problem in [27]. However, naively applying aforementioned classic approximation schemes fails to preserve such structures. To remedy this, we introduce a new scheme to approximate maps whose values are points on a *Riemannian manifold*. Our scheme works by pulling back the approximation problem to the tangent space. In this way, the problem is reduced again to the classic function approximation problem between vector spaces. Consequently, our scheme can leverage all of the previously mentioned classic techniques.

A pullback to a tangent space is a natural idea to solve problems on manifolds

***Funding:** This project was funded by BOF project C16/21/002 by the Internal Funds KU Leuven and FWO project G080822N. J. Van der Veken is additionally supported by the Research Foundation–Flanders (FWO) and the Fonds de la Recherche Scientifique (FNRS) under EOS Project G0I2222N. R. Vandebril is additionally supported by the Fund for Scientific Research–Flanders (Belgium), projects G0A9923N and G0B0123N.

[†]KU Leuven, Department of Computer Science, Celestijnenlaan 200A – box 2402, B-3000 Leuven, Belgium (simon.jacobsson@kuleuven.be)

[‡]KU Leuven, Department of Computer Science, Celestijnenlaan 200A – box 2402, B-3000 Leuven, Belgium (raf.vandebril@kuleuven.be)

[§]KU Leuven, Department of Mathematics, Celestijnenlaan 200B – box 2400, B-3000, Leuven, Belgium (joeri.vanderveken@kuleuven.be)

[¶]KU Leuven, Department of Computer Science, Celestijnenlaan 200A – box 2402, B-3000 Leuven, Belgium (nick.vannieuwenhoven@kuleuven.be); Leuven.AI – KU Leuven Institute for AI, B-3000 Leuven, Belgium,

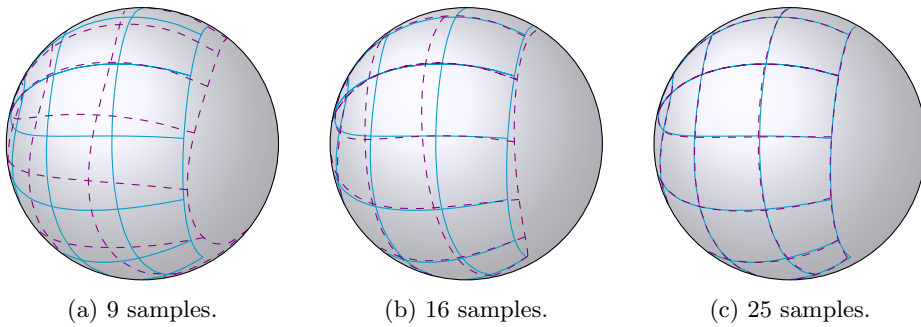


Fig. 1.1: Using different number of samples, we approximate $f: [-1, 1]^2 \rightarrow S^2$. Let Γ be a 10×10 grid on $[-1, 1]^2$. Solid lines show $f(\Gamma)$ and dashed lines show $\hat{f}(\Gamma)$.

in general. In the context of interpolation, some previous related work based on this idea is for example Zimmermann [68] and Zimmermann and Bergmann [70], who solve uni- and multivariate Hermite interpolation problems on manifolds. Bergmann and Gousenbourger [11] and Gousenbourger, Massart, and Absil [33] define manifold-valued generalizations of Bézier curves. While these schemes could be used in some cases to approximate maps into manifolds, they were designed as interpolation methods. We focus on *approximation* rather than interpolation.

1.1. Contribution. We propose to approximate a map $f: R \rightarrow M$, where R may be an arbitrary space and M is a Riemannian manifold, by a natural, generally applicable three-step template:

1. Choose a point $p \in M$ from which to linearize the approximation problem.
2. Pull f back to the tangent space $T_p M$ using a *normal coordinate chart* [44], and approximate the resulting map $g := \log_p \circ f: R \rightarrow T_p M$ by $\hat{g}: R \rightarrow T_p M$ using an arbitrary approximation scheme for maps into vector spaces.
3. Push \hat{g} forward with \exp_p to yield $\hat{f} := \exp_p \circ \hat{g}: R \rightarrow M$.

Alternatively, if \exp_p and \log_p are not known explicitly, a *retraction* [1, 15] may be used instead. Algorithm 4.1 is a detailed description of a concrete algorithm that results from applying this template to maps with domain $R = [-1, 1]^m$.

Figure 1.1 is a small example of Algorithm 4.1 approximating a map into the sphere S^2 , defined by stereographic projection of $(x, y) \mapsto (x^2 - y^2, 2xy)$.

While the proposed template is conceptually straightforward, the main challenge is establishing a bound on the approximation error, as any discrepancy between g and \hat{g} will be propagated through the exponential map. This requires understanding how the endpoint of a geodesic, which is a solution of a particular initial value problem on a manifold, changes as the initial conditions of this differential equation are varied. Theorem 3.1 shows how *Toponogov's theorem* can be leveraged to derive upper bounds on this perturbation.

1.2. Outline. Toponogov's theorem is a well-known Riemannian comparison theorem. In section 2, we recall some geometric preliminaries to be able to utilize it.

Section 3 describes the error analysis of our algorithm template, where our main original contribution is Theorem 3.1. Our analysis assumes a lower bound on the *sectional curvature* of the manifold. For completeness and ease of reference, we lists

several concrete manifolds along with explicit bounds on their curvature in [Appendix A](#). We are especially interested in manifolds with nonnegative curvature, as their error bound is guaranteed not to be worse than in the familiar linear case.

Inspired by Dolgov, Kressner, and Strössner [58] and by Strössner, Sun, and Kressner [57], we use *tensorized Chebyshev interpolation* in step 2 of our template to implement [Algorithm 4.1](#). We discuss the rest of the implementation details and recall error bounds for tensorized Chebyshev interpolation in [section 4](#).

We present two example approximation problems inspired by linear algebra applications in [section 5](#). In these examples, the approximation error is verified to be bounded by [Theorem 3.1](#). Our implementation is available as a Julia package, `ManiFactor.jl` [40].

Finally, the paper is concluded with a summary of the main results and a future outlook in [section 6](#).

Acknowledgements. We thank Arne Bouillon for spotting an error in (3.5) in an earlier draft, and Astrid Herremans for her expertise in approximation theory and her suggestions about the figures.

Notation. The following notation will be used throughout the paper:

- $\text{id}: V \rightarrow V$ is the *identity map*.
- $\|\cdot\|_\infty$ is the *infinity norm*. For arrays $A \in \mathbb{R}^{N_1 \times \dots \times N_m}$, it is defined as the element with maximum absolute value. For functions $g: R \rightarrow \mathbb{R}$, it is defined as $\sup_{x \in R} |g(x)|$. If O is an operator, we will also use $\|O\|_\infty$ to mean the operator norm with respect to the infinity norm.
- $\angle(u, v)$ is the *angle* between two vectors u and v in an inner product space $(V, \langle \cdot, \cdot \rangle)$ with induced norm $\|\cdot\|$. It is defined as $\arccos(\langle u/\|u\|, v/\|v\| \rangle)$.
- For a Riemannian manifold M , $\langle \cdot, \cdot \rangle_p$ is the inner product on the tangent space $T_p M$ at $p \in M$, $\|\cdot\|_p$ is the induced norm on $T_p M$, and $d_M(\cdot, \cdot)$ is the induced geodesic distance on M . \exp_p and \log_p are the exponential and logarithmic maps at p respectively.

2. Geometric preliminaries. We now present a high-level overview of the key concepts from Riemannian geometry that we will use. The technical details, which the present work does not require, can be found in standard references, such as Lee [43, 44].

Manifolds are abundant in numerical analysis. Examples are sets of orthogonal matrices, positive definite matrices, upper triangular matrices, tensors of fixed rank, and linear subspaces of fixed dimension. Morally, a *manifold* is a space M that locally can be identified with open subsets of \mathbb{R}^n . Such an identification is called a *chart*. A detailed introduction to manifolds can be found in Lee [43, chapters 1–3].

A *Riemannian manifold* M is a manifold with a notion of distance between points. A *geodesic* is a curve in M that is locally distance-minimizing. The *tangent space* $T_p M$ to M at a point $p \in M$ is the space of velocity vectors of curves in M through p . It is an n -dimensional vector space. Each tangent vector is associated with a geodesic through p , and vice versa. This gives a canonical chart around each point $p \in M$, called a *normal coordinate chart*. It consists of the *manifold exponential* and its inverse, the *manifold logarithm*, which identify a neighbourhood $S \subset T_p M$ of 0 with a neighbourhood $S' \subset M$ of p . We denote them by

$$(2.1) \quad \exp_p: S \rightarrow S', \quad \text{and} \quad \log_p: S' \rightarrow S.$$

A detailed introduction to Riemannian geometry is given in Lee [44, chapters 1–8].

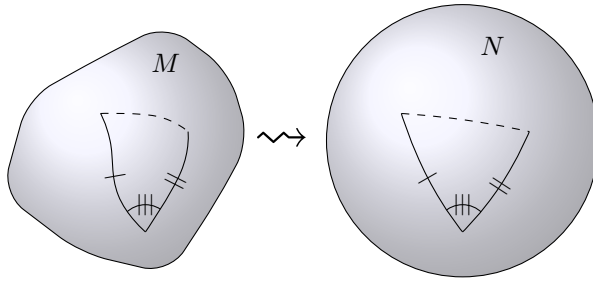


Fig. 2.1: **Proposition 2.1** gives conditions for which the length of the opposite (dashed) side in M is bounded by the length of the opposite (dashed) side in N . Equal length geodesics and equal angles have the same number of notches.

A Riemannian manifold M is *geodesically convex* if for any two points on M , there is a unique distance-minimizing geodesic connecting them. Such a geodesic is called *minimal*. A *geodesic triangle* is a set of three minimal geodesics connecting three points on M .

A *Lie group* is a manifold equipped with a group operation. Specifically, Riemannian Lie groups whose group operation is compatible with their metric have many desirable properties. They thus form a main class of examples in [Appendix A](#). A concise introduction to Lie groups can be found in Arvanitoyeorgos [6].

2.1. Sectional curvature. If M is a two-dimensional Riemannian manifold, then we can define the *Gaussian curvature* K at a point $p \in M$ in several ways. One way is to define it by the angular defect of small triangles:

$$(2.2) \quad \alpha + \beta + \gamma - \pi = KA + \text{higher order terms},$$

where α, β, γ are the angles of a geodesic triangle in M at p with area A .

If M is not two-dimensional, consider a two-dimensional linear subspace Π of $T_p M$. Then $\Sigma = \exp_p(\Pi)$ is a two-dimensional submanifold of M . The Gaussian curvature of Σ at p is called the *sectional curvature* of M along Π .

A manifold with constant sectional curvature H is called a *model manifold*. It is uniquely determined by H and its dimension.

2.2. Riemannian comparison theory. Riemannian comparison theory studies inequalities involving geometric quantities. A good reference is Cheeger and Ebin [21]. Many comparison theorems relate properties of geodesics to curvature bounds. *Toponogov's theorem* is such a theorem, bounding side lengths of geodesic triangles defined on manifolds with lower bounded sectional curvature. It is illustrated in [Figure 2.1](#).

PROPOSITION 2.1 (Toponogov's theorem [21, Theorem 2.2]). *Let M be a geodesically convex Riemannian manifold with sectional curvature bounded from below by some constant H . Let $\gamma_1, \gamma_2: [0, 1] \rightarrow M$ be minimal geodesics such that $\gamma_1(0) = \gamma_2(0)$. If $H > 0$, also assume that $d_M(\gamma_1(0), \gamma_1(1)), d_M(\gamma_2(0), \gamma_2(1)) \leq \frac{\pi}{\sqrt{H}}$. Consider a model manifold N of constant sectional curvature H and let $\lambda_1, \lambda_2: [0, 1] \rightarrow N$ be geodesics such that $\lambda_1(0) = \lambda_2(0)$ and the angle where they meet satisfies $\angle(\lambda_1, \lambda_2) = \angle(\gamma_1, \gamma_2)$. Then*

$$(2.3) \quad d_M(\gamma_1(1), \gamma_2(1)) \leq d_N(\lambda_1(1), \lambda_2(1)).$$

The advantage of looking at geodesic triangles on the model manifold is that there are spherical and hyperbolic versions of the trigonometric identities. These identities are used in [section 3](#) to find explicit error bounds when approximating maps into manifolds.

LEMMA 2.2 (Reid [50, sections 3.2 and 3.10]). *Let N be a manifold of constant sectional curvature H and consider a geodesic triangle on N with side lengths A , B , C and opposite angles a , b , c respectively. Then*

$$(2.4) \quad \cos(C\sqrt{H}) = \cos(A\sqrt{H})\cos(B\sqrt{H}) + \sin(A\sqrt{H})\sin(B\sqrt{H})\cos c$$

if $H > 0$, and

$$(2.5) \quad \cosh(C\sqrt{|H|}) = \cosh(A\sqrt{|H|})\cosh(B\sqrt{|H|}) - \sinh(A\sqrt{|H|})\sinh(B\sqrt{|H|})\cos c$$

if $H < 0$.

3. Error analysis. The distance between two points on a Riemannian manifold depends on the geometry of that manifold. For example, the distance between two orthogonal matrices A and B in the space of orthogonal matrices will always be greater than or equal to the distance between A and B in the ambient space of matrices. When approximating maps into Riemannian manifolds it is natural to measure the approximation error *intrinsically* on the manifold, rather than in some *extrinsic* ambient space in which the manifold could be embedded. Moreover, for embedded manifolds with large codimension, such as low-rank matrices or tensors, it can be inefficient or even infeasible to measure the error in the ambient space. The next result thus bounds the intrinsic error of the approximation template from [subsection 1.1](#).

THEOREM 3.1. *Let M be a geodesically convex Riemannian manifold with sectional curvature bounded from below by some constant H and let $f: R \rightarrow M$, where R is an arbitrary set such that its image fits in a single normal coordinate chart $S \subset T_p M$ around $p \in M$. Assume that the elements in S have norm bounded by some constant σ . Let*

$$(3.1) \quad g = \log_p \circ f: R \rightarrow S \quad \text{and} \quad \hat{f} = \exp_p \circ \hat{g}: R \rightarrow M,$$

where $\hat{g}: R \rightarrow S$ is an approximation of g such that

$$(3.2) \quad \|g(x) - \hat{g}(x)\|_p \leq \epsilon$$

for all $x \in R$. Then, the distance between $f(x)$ and $\hat{f}(x)$ on M obeys

$$(3.3) \quad d_M(f(x), \hat{f}(x)) \leq \epsilon \quad \text{if } H \geq 0,$$

$$(3.4) \quad d_M(f(x), \hat{f}(x)) \leq \epsilon + \frac{2}{\sqrt{|H|}} \operatorname{arcsinh} \frac{\epsilon \sinh(\sigma\sqrt{|H|})}{2\sigma} \quad \text{if } H < 0,$$

for all $x \in R$.

Remark 3.2. We can in turn upper bound (3.4) by

$$(3.5) \quad d_M(f(x), \hat{f}(x)) \leq \epsilon + \frac{2}{\sqrt{|H|}} \log \left(\frac{\epsilon \exp(\sigma\sqrt{|H|})}{2\sigma} + 1 \right).$$

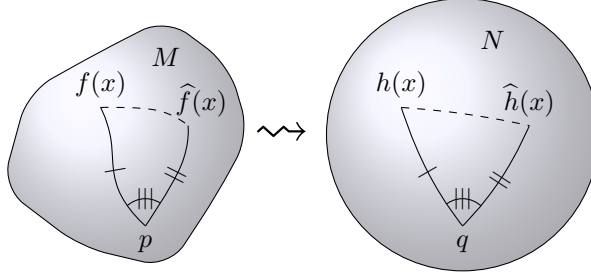


Fig. 3.1: Geodesic triangles defined by p , f , and \hat{f} . The map from M to N is $\exp_{N,q} \circ \log_{M,p}$.

The assumptions in [Theorem 3.1](#) about geodesic convexity, bounded curvature, and bounded normal coordinate chart may seem very specific, but we note that they are always satisfied in some neighbourhood of p . To formulate explicit bounds, we however need explicit expressions for H . Therefore, we list several standard manifolds along with explicit lower bounds for their sectional curvature in [Appendix A](#).

Proof of Theorem 3.1. The proof can be summarized as applying Toponogov's theorem to the geodesic triangle $(f(x), \hat{f}(x), p)$, as visualized in [Figure 3.1](#).

Let N be the manifold of constant curvature H and let $q \in N$. Fix some isometry $T_p M \sim T_q N$ and let $\exp_{N,q}: S \rightarrow N$ be the manifold exponential on N . Define $h = \exp_{N,q} \circ g$ and $\hat{h} = \exp_{N,q} \circ \hat{g}$. By [Proposition 2.1](#),

$$(3.6) \quad d_M(f(x), \hat{f}(x)) \leq d_N(h(x), \hat{h}(x)).$$

Now our task is to bound the right-hand side of this inequality.

For brevity, from now on we drop the argument x of the functions f , g , and h .

Case 1: $H \geq 0$. Without loss of generality, let $H = 0$. Then $N = T_p M$ and so

$$(3.7) \quad d_N(h, \hat{h}) = \|g - \hat{g}\|_p \leq \epsilon.$$

Case 2: $H < 0$. Consider the geodesic triangle $(h(x), \hat{h}(x), q)$. Define $c(t) = \cosh(t\sqrt{|H|})$ and $s(t) = \sinh(t\sqrt{|H|})$. Then [Lemma 2.2](#) says that

$$(3.8) \quad c(d(h, \hat{h})) = c(\|g\|_p)c(\|\hat{g}\|_p) - s(\|g\|_p)s(\|\hat{g}\|_p) \cos(\angle(g, \hat{g})).$$

Since \sinh is positive on \mathbb{R}^+ ,

$$(3.9) \quad s(\|g\|_p)s(\|\hat{g}\|_p) \geq 0.$$

Hence using

$$(3.10) \quad \cos(\angle(g, \hat{g})) = \frac{\langle g, \hat{g} \rangle_p}{\|g\|_p \|\hat{g}\|_p} = \frac{\|g\|_p^2 + \|\hat{g}\|_p^2}{2\|g\|_p \|\hat{g}\|_p} - \frac{\|g - \hat{g}\|_p^2}{2\|g\|_p \|\hat{g}\|_p} \geq 1 - \frac{\|g - \hat{g}\|_p^2}{2\|g\|_p \|\hat{g}\|_p}$$

in (3.8) gives us

$$(3.11) \quad c(d(h, \hat{h})) \leq c(\|g\|_p)c(\|\hat{g}\|_p) - s(\|g\|_p)s(\|\hat{g}\|_p) \left(1 - \frac{\|g - \hat{g}\|_p^2}{2\|g\|_p\|\hat{g}\|_p}\right)$$

$$(3.12) \quad = c(\|g\|_p - \|\hat{g}\|_p) + \frac{\|g - \hat{g}\|_p^2 s(\|g\|_p)s(\|\hat{g}\|_p)}{2\|g\|_p\|\hat{g}\|_p}.$$

Since \cosh is even and increasing on \mathbb{R}^+ , we may use the reverse triangle inequality to see that

$$(3.13) \quad c(d(h, \hat{h})) \leq c(\|g - \hat{g}\|_p) + \frac{\|g - \hat{g}\|_p^2 s(\|g\|_p)s(\|\hat{g}\|_p)}{2\|g\|_p\|\hat{g}\|_p}.$$

Furthermore, noting that $\frac{\sinh x}{x}$ is increasing and positive on \mathbb{R}^+ , we have that

$$(3.14) \quad c(d(h, \hat{h})) \leq c(\|g - \hat{g}\|_p) + \frac{\|g - \hat{g}\|_p^2 s(\sigma)^2}{2\sigma^2}.$$

This is equivalent to

$$(3.15) \quad 1 + 2s\left(\frac{d(h, \hat{h})}{2}\right)^2 \leq 1 + 2s\left(\frac{\|g - \hat{g}\|_p}{2}\right)^2 + \frac{\|g - \hat{g}\|_p^2 s(\sigma)^2}{2\sigma^2},$$

so that

$$(3.16) \quad d(h, \hat{h}) \leq 2s^{-1}\left(\sqrt{s\left(\frac{\|g - \hat{g}\|_p}{2}\right)^2 + \frac{\|g - \hat{g}\|_p^2 s(\sigma)^2}{4\sigma^2}}\right),$$

and since \sinh , $\operatorname{arcsinh}$, \cdot^2 , and $\sqrt{\cdot}$ are all increasing on \mathbb{R}^+ , we find

$$(3.17) \quad d(h, \hat{h}) \leq 2s^{-1}\left(\sqrt{s\left(\frac{\epsilon}{2}\right)^2 + \frac{\epsilon^2 s(\sigma)^2}{4\sigma^2}}\right).$$

Lastly we will use that concave functions are *subadditive*, $\sqrt{a^2 + b^2} \leq a + b$ and $\operatorname{arcsinh}(\sinh a + \sinh b) \leq a + b$ for nonnegative a and b . Thus

$$(3.18) \quad d(h, \hat{h}) \leq \epsilon + 2s^{-1}\left(\frac{\epsilon s(\sigma)}{2\sigma}\right).$$

This concludes the proof. \square

If the exponential or logarithmic map are not explicitly known for a manifold, then we might still be able to proceed by using a *retraction*. This is an injective map r_p that approximates the exponential map at p . For a precise definition, see Absil, Mahony, and Sepulchre [1, Definition 4.1.1].

Assume the same conditions as in [Theorem 3.1](#). Moreover, assume the max error between r_p and \exp_p is bounded by ζ , assume the max error between r_p^{-1} and \log_p is bounded by η , and assume that the vector-valued approximation scheme $\mathcal{I}: g \mapsto \hat{g}$ is \mathbb{R} -linear and that its operator infinity norm is Λ . Now, instead of using

$\widehat{f} = (\exp_p \circ \mathcal{I} \circ \log_p)(f)$, we use $\widehat{f} = (r_p \circ \mathcal{I} \circ r_p^{-1})(f)$. It is then straightforward to show the following bounds:

(3.19)

$$d_M(f(x), \widehat{f}(x)) \leq \epsilon + \Lambda\eta + \zeta \quad \text{if } H \geq 0,$$

(3.20)

$$d_M(f(x), \widehat{f}(x)) \leq \epsilon + \Lambda\eta + \zeta + \frac{2}{\sqrt{|H|}} \operatorname{arcsinh} \left(\frac{(\epsilon + \Lambda\eta) \sinh(\sigma\sqrt{|H|})}{2\sigma} \right) \quad \text{if } H < 0.$$

When $H \rightarrow 0^-$, (3.4) tends to

$$(3.21) \quad d_M(f, \widehat{f}) \leq 2\epsilon,$$

which shows that it is not a tight bound. To explain why, first note that (3.10) is an equality when $\|g(x)\|_p = \|\widehat{g}(x)\|_p$, but we also used the reverse triangle inequality in (3.13) which is an equality when g and \widehat{g} are collinear. Furthermore, in (3.18) we used subadditivity for the square root, which is an equality only when one of the terms is 0. But for small curvatures and small ϵ , the two terms in (3.18) are approximately equal. One could say that we lost a factor $\sqrt{2}$ in each of these steps.

Even though the bound (3.4) is not tight, there is, in the following sense, no better bound.

PROPOSITION 3.3. *Recall the notation of Theorem 3.1. Assume that M has constant negative sectional curvature H and let \widehat{g} be an approximation to g such that the maximum error ϵ is attained at a point $x \in R$ with $\|\widehat{g}(x)\|_p = \|g(x)\|_p = \sigma$. Then*

$$(3.22) \quad d_M(f(x), \widehat{f}(x)) = \frac{2}{\sqrt{|H|}} \operatorname{arcsinh} \left(\frac{\epsilon \sinh(\sigma\sqrt{|H|})}{2\sigma} \right).$$

Proof. Consider again the proof of Theorem 3.1. If $\|g\|_p = \|\widehat{g}\|_p$, then (3.10) is an equality, and we do not need to use the reverse triangle inequality in (3.13), hence (3.15) reduces to

$$(3.23) \quad 1 + 2s \left(\frac{d_M(f, \widehat{f})}{2} \right)^2 = 1 + \frac{\epsilon^2 s(\sigma)^2}{2\sigma^2}.$$

This is equivalent to what we wanted to prove. \square

As an immediate consequence of Theorem 3.1 we can obtain bounds on the propagation of a small perturbation of a tangent vector through the exponential map \exp_p . The size of this output perturbation relative to the input perturbation is quantified by the *condition number*. Recall the definition of Rice's condition number [51] of a map $\phi: A \rightarrow B$ between metric spaces (A, d_A) and (B, d_B) :

$$(3.24) \quad \kappa[\phi](x) = \limsup_{\substack{x' \in A, \\ d_A(x, x') \rightarrow 0}} \frac{d_B(\phi(x), \phi(x'))}{d_A(x, x')}.$$

Let $\phi = \exp_p: (R \rightarrow S) \rightarrow (R \rightarrow M)$, with the metrics

(3.25)

$$d_{R \rightarrow S}(g, \widehat{g}) = \sup_{x \in R} \|g(x) - \widehat{g}(x)\|_p, \quad \text{and} \quad d_{R \rightarrow M}(f, \widehat{f}) = \sup_{x \in R} d_M(f(x), \widehat{f}(x)).$$

The condition number implies an asymptotically sharp error bound

$$(3.26) \quad d_{R \rightarrow M}(\exp_p \circ g, \exp_p \circ \widehat{g}) \leq \kappa[\exp_p](g) d_{R \rightarrow S}(g, \widehat{g}) + o(d_{R \rightarrow S}(g, \widehat{g}))$$

$$(3.27) \quad = \kappa[\exp_p](g)\epsilon + o(\epsilon),$$

We obtain the following corollary of [Theorem 3.1](#) and [Proposition 3.3](#).

COROLLARY 3.4. *Recall the notation of [Theorem 3.1](#). The condition number κ of the map $g \mapsto f$ satisfies*

$$(3.28) \quad 1 \leq \kappa \leq 1 + \frac{\sinh(\sigma\sqrt{|H|})}{\sigma\sqrt{|H|}} \quad \text{if } H < 0,$$

$$(3.29) \quad \kappa = 1 \quad \text{if } H \geq 0.$$

Furthermore, if M is a model manifold with constant negative sectional curvature H , then it is also lower bounded by

$$(3.30) \quad \frac{\sinh(\sigma\sqrt{|H|})}{\sigma\sqrt{|H|}} \leq \kappa.$$

The condition number grows exponentially in both σ and $\sqrt{|H|}$. For example, such innocent looking parameters as $H = -10$ and $\sigma = 10$ gives a condition number of almost $9 \cdot 10^{11}$, potentially losing about 12 digits of accuracy. In general, if we want to be guaranteed a reasonable condition number, we should make sure that the inputs have small norm: $\sigma \leq \frac{1}{\sqrt{|H|}}$.

4. A concrete implementation. Henceforth, we want to approximate a function $f: [-1, 1]^m \rightarrow M$, where M is a Riemannian manifold. In the notation of [section 3](#), $R = [-1, 1]^m$. In this section, we present a concrete realization of the approximation template discussed in [subsection 1.1](#), using tensorized Chebyshev interpolation. It is presented as [Algorithm 4.1](#). We describe steps 1 and 2 of the template in detail. The final step consists of applying the exponential map to the constructed approximation, which requires no further discussion.

4.1. Choosing from where to linearize. In practice, the choice of the point $p \in M$ in [Theorem 3.1](#) affects the error a lot. Because the radius σ of the chart S appears as an exponent in the error bound [\(3.4\)](#), it is natural to try to minimize it. However, direct minimization of σ is a nontrivial Riemannian optimization problem, so instead we consider an approximation. Consider a sequence $(\xi_i)_{i=1}^N$ of points in R , sampled independently from the same distribution on R . Then, consider the total squared distance to p ,

$$(4.1) \quad \sum_{i=1}^N d_M(f(\xi_i), p)^2.$$

The idea is that [\(4.1\)](#) may be easier to minimize than σ itself, while they are correlated. A p that minimizes [\(4.1\)](#) is called a *Riemannian center of mass* of $(f(\xi_i))_{i=1}^N$ [\[41\]](#). An efficient way to approximate a Riemannian center of mass is by successive geodesic interpolation [\[18, 19, 20, 22\]](#), namely

$$(4.2) \quad m(p_1) = p_1,$$

$$(4.3) \quad m(p_1, \dots, p_N) = \exp_{p_N} \left(\frac{N-1}{N} \log_{p_N} m(p_1, \dots, p_{N-1}) \right).$$

Algorithm 4.1 For approximating maps into manifolds.

Require: $f: [-1, 1]^m \rightarrow M$, number $N_k + 1$ of Chebyshev nodes to use in each direction $k = 1, \dots, m$.

Ensure: Approximant $\hat{f}: [-1, 1]^m \rightarrow M$ of f satisfies the error bound of [Theorem 3.1](#).

- 1: Choose $p \in M$ as (an approximation of) the Karcher mean of a large number of $f(x)$ for x chosen from a uniform distribution on $[-1, 1]^m$.
- 2: Let $g = \log_p \circ f$.
- 3: **for** $k = 1, \dots, m$ **do**
- 4: **for** $i_k = 1, \dots, N_k + 1$ **do**
- 5: Let $t_{i_k} = \cos\{(2i_k - 1)\pi/2(N_k + 1)\}$ be the i_k th Chebyshev node.
- 6: **for** $j = 1, \dots, n$ **do**
- 7: Let $G_{i_1 \dots i_m j} = g_j(t_{i_1}, \dots, t_{i_m})$.
- 8: **end for**
- 9: **end for**
- 10: **end for**
- 11: Let $G_{i_1 \dots i_m j} = \sum_{a_1, \dots, a_m, b} C_{a_1 \dots a_m b} U_{i_1 a_1}^{(1)} \dots U_{i_m a_m}^{(m)} V_{bj}$ be an ST-HOSVD of G .
- 12: **for** $k = 1, \dots, m$ **do**
- 13: Let $\hat{h}_{a_k}^{(k)}$ be the degree- N_k interpolating polynomial satisfying $\hat{h}_{a_k}^{(k)}(t_{i_k}) = U_{i_k a_k}^{(k)}$.
- 14: **end for**
- 15: **for** $j = 1, \dots, n$ **do**
- 16: Let $\hat{g}_j(x) = \sum_{a_1, \dots, a_m, b} C_{a_1 \dots a_m b} \hat{h}_{a_1}^{(1)}(x_1) \dots \hat{h}_{a_m}^{(m)}(x_m) V_{bj}$.
- 17: **end for**
- 18: Let $\hat{f} = \exp_p \circ \hat{g}$.
- 19: return \hat{f} .

Note that, in the Euclidean case, $m(p_1, \dots, p_N)$ is the arithmetic mean of $(p_i)_{i=1}^N$, and is thus exactly the Riemannian center of mass.

In our implementation, we choose p as $m(f(\xi_1), \dots, f(\xi_N))$ with $(\xi_i)_{i=1}^N$ sampled from a uniform distribution on R .

4.2. Tensorized Chebyshev interpolation. For the second step in our implementation, we choose *tensorized Chebyshev interpolation*.

Tensorizing a univariate approximation scheme is a standard approach for multivariate approximation. Here, we first recall Schultz's [53] approach, specialized to the case of a linear approximation scheme. Let $\mathcal{I}: ([-1, 1] \rightarrow \mathbb{R}) \rightarrow ([-1, 1] \rightarrow \mathbb{R})$ be a *linear evaluation-based scheme* for approximating real univariate functions; that is,

1. \mathcal{I} is a linear map: $\mathcal{I}(\alpha f + \beta g) = \alpha \mathcal{I}(f) + \beta \mathcal{I}(g)$ for all real univariate functions f and g and for all real numbers α and β .
2. $\mathcal{I} = \mathcal{F} \circ \mathcal{E}_P$, where $\mathcal{F}: \mathbb{R}^N \rightarrow ([-1, 1] \rightarrow \mathbb{R})$ is linear and $\mathcal{E}_P: ([-1, 1] \rightarrow \mathbb{R}) \rightarrow \mathbb{R}^N$ is the *evaluation map* that takes a function f and maps it to its evaluations $(f(x_1), \dots, f(x_N))$ in the sample points $P = (x_1, \dots, x_N) \in [-1, 1]^N$.

Then, the *tensor product* $\mathcal{I} \otimes \dots \otimes \mathcal{I}$ is well defined. Recall the definition of the tensor product of linear maps [36]. Let $U_1, \dots, U_m, V_1, \dots, V_m$ be vector spaces. Given linear maps $L_1: U_1 \rightarrow V_1, \dots, L_m: U_m \rightarrow V_m$, their tensor product is the unique

linear map that satisfies

$$(4.4) \quad \begin{aligned} L_1 \otimes \cdots \otimes L_m : U_1 \otimes \cdots \otimes U_m &\rightarrow V_1 \otimes \cdots \otimes V_m, \\ u_1 \otimes \cdots \otimes u_m &\mapsto L_1(u_1) \otimes \cdots \otimes L_m(u_m), \end{aligned}$$

for all pure tensors $u_1 \otimes \cdots \otimes u_m$. The following result bounds the error of a tensorized univariate approximation scheme.

LEMMA 4.1 (Essentially, Schultz [53, Theorem 2.1]). *Let $g: [-1, 1]^m \rightarrow \mathbb{R}$. For each $k = 1, \dots, m$, let $\mathcal{I}_k = \mathcal{F}_k \circ \mathcal{E}_{P_k}$ be a linear evaluation-based approximation scheme using the N_k evaluation points P_k on $[-1, 1]$. Consider g as a map of the k th argument only, i.e., $h_k(t) = g(x_1, \dots, x_{k-1}, t, x_{k+1}, \dots, x_m)$ and assume that*

$$(4.5) \quad |h_k(t) - \mathcal{I}_k(h_k)(t)| \leq \epsilon_k$$

for all $t \in [-1, 1]$ and for all $x \in [-1, 1]^m$. Let

$$(4.6) \quad G = (\mathcal{E}_{P_1} \otimes \cdots \otimes \mathcal{E}_{P_m})g \in \mathbb{R}^{N_1 \times \cdots \times N_m}$$

be the tensor obtained from evaluating g on the product grid $P_1 \times \cdots \times P_m$. Furthermore, let $\widehat{G} = G + E$ for some E . If $\widehat{g} = (\mathcal{F}_1 \otimes \cdots \otimes \mathcal{F}_m)\widehat{G}$, then

$$(4.7) \quad \|g - \widehat{g}\|_\infty \leq \epsilon_1 + \Lambda_1 \epsilon_2 + \cdots + \Lambda_1 \cdots \Lambda_{m-1} \epsilon_m + \Lambda_1 \cdots \Lambda_m \|E\|_\infty,$$

where $\Lambda_k = \|\mathcal{F}_k\|_\infty$.

Proof. We have

$$(4.8) \quad \begin{aligned} \|\widehat{g} - g\|_\infty &= \|(\mathcal{F}_1 \otimes \cdots \otimes \mathcal{F}_m)(G + E) - g\|_\infty \\ &\leq \|(\mathcal{F}_1 \otimes \cdots \otimes \mathcal{F}_m)G - g\|_\infty + \|(\mathcal{F}_1 \otimes \cdots \otimes \mathcal{F}_m)E\|_\infty \\ &\leq \|(\mathcal{I}_1 \otimes \cdots \otimes \mathcal{I}_m)g - g\|_\infty + \Lambda_1 \cdots \Lambda_m \|E\|_\infty. \end{aligned}$$

The first term is bounded as in [53, Theorem 2.1], concluding the proof. \square

Recall that Chebyshev polynomial interpolation interpolates a function on $[-1, 1]$ in the *Chebyshev nodes* $\cos((2k-1)\pi/2n)$, $k = 1, \dots, n$. Chebyshev interpolants have many nice properties. Specifically, their approximation error is bounded, see, e.g., Trefethen [62, Theorems 7.2 and 8.2], and the operator norm of Chebyshev interpolation is also bounded, see, e.g., Trefethen [62, Theorem 15.2]. Combining Lemma 4.1 with these bounds gives a concrete error bound for tensorized Chebyshev interpolation.

COROLLARY 4.2. *Recall the notation of Lemma 4.1. If g has absolutely continuous partial derivatives along x_k up to order $\nu_k - 1$ and the total variation of g 's partial derivative of order ν_k along x_k is bounded by V_k , then*

$$(4.9) \quad \begin{aligned} \|g - \widehat{g}\|_\infty &\leq \frac{4V_1}{\pi\nu_1(N_1 - \nu_1)^{\nu_1}} + \frac{4\Lambda_{N_1}V_2}{\pi\nu_2(N_2 - \nu_2)^{\nu_2}} + \cdots + \frac{4\Lambda_{N_1} \cdots \Lambda_{N_{m-1}}V_m}{\pi\nu_m(N_m - \nu_m)^{\nu_m}} \\ &\quad + \Lambda_{N_1} \cdots \Lambda_{N_m} \|E\|_\infty, \end{aligned}$$

where $\Lambda_{N_k} \leq \frac{2}{\pi} \log(N_k + 1) + 1$. Especially, if $N_1 = \cdots = N_m = N$, $\nu_1 = \cdots = \nu_m = \nu$, and $V_1 = \cdots = V_m = V$, then

$$(4.10) \quad \|g - \widehat{g}\|_\infty \leq \frac{4(\Lambda_N^m - 1)V}{\pi\nu(N - \nu)^\nu(\Lambda_N - 1)} + \Lambda_N^m \|E\|_\infty.$$

COROLLARY 4.3. Recall the notation of Lemma 4.1. If g is analytic in x_k with an analytic continuation inside the Bernstein ellipse $(\rho_k e^{i\theta} + \rho_k^{-1} e^{-i\theta})/2$ bounded by C_k , then

$$(4.11) \quad \|g - \hat{g}\|_\infty \leq \frac{4C_1}{(\rho_1 - 1)\rho_1^{N_1}} + \frac{4\Lambda_{N_1}C_2}{(\rho_2 - 1)\rho_2^{N_2}} + \cdots + \frac{4\Lambda_{N_1} \cdots \Lambda_{N_{m-1}}C_m}{(\rho_m - 1)\rho_m^{N_m}} + \Lambda_{N_1} \cdots \Lambda_{N_m} \|E\|_\infty,$$

where $\Lambda_{N_k} \leq \frac{2}{\pi} \log(N_k + 1) + 1$. Especially, if $N_1 = \cdots = N_m = N$, $\rho_1 = \cdots = \rho = \rho$, and $C_1 = \cdots = C_m = C$, then

$$(4.12) \quad \|g - \hat{g}\|_\infty \leq \frac{4(\Lambda_N^m - 1)C}{(\rho - 1)\rho^N(\Lambda_N - 1)} + \Lambda_N^m \|E\|_\infty.$$

Note that these bounds for tensorized Chebyshev approximation are slightly better than those obtained by Mason [45, (21) and (22)]. In particular, tensorized Chebyshev approximation yields quasi-optimal approximations of continuous functions by bounded-degree polynomials [45].

The approximation \hat{g} in Lemma 4.1 is defined as applying the multilinear map $\mathcal{F}_1 \otimes \cdots \otimes \mathcal{F}_m$ to the tensor of function evaluations G . Unfortunately, this suffers from the curse of dimensionality because it requires access to all $N_1 \cdots N_m$ entries of G . To mitigate it, a common assumption is that the function evaluations G can be well approximated by a tensor $\hat{G} \in \mathbb{R}^{N_1 \times \cdots \times N_m} \sim \mathbb{R}^{N_1} \otimes \cdots \otimes \mathbb{R}^{N_m}$ that admits a data-sparse tensor decomposition.

Consider, for example, a Tucker decomposition [63] $\hat{G} = (U^{(1)} \otimes \cdots \otimes U^{(m)})C$, where $C \in \mathbb{R}^{r_1} \otimes \cdots \otimes \mathbb{R}^{r_m}$ and each $U^{(k)}: \mathbb{R}^{r_k} \rightarrow \mathbb{R}^{N_k}$, $k = 1, \dots, m$, is a linear map, or, in coordinates, an $N_k \times r_k$ matrix. Discrete tensors containing smooth function evaluations can be well approximated with a Tucker decomposition with small r_k 's [54]. Given such a Tucker decomposition of G , we can construct \hat{g} as

$$(4.13) \quad \hat{g}(x) = (\mathcal{F}_1 \otimes \cdots \otimes \mathcal{F}_m)((U^{(1)} \otimes \cdots \otimes U^{(m)})C)(x)$$

$$(4.14) \quad = \sum_{a_1=1}^{r_1} \cdots \sum_{a_m=1}^{r_m} C_{a_1 \dots a_m} \mathcal{F}_1(U_{:a_1}^{(1)})(x_1) \cdots \mathcal{F}_m(U_{:a_m}^{(m)})(x_m),$$

where $U_{:a}^{(k)} \in \mathbb{R}^{N_k}$ is the a th column of $U^{(k)} \in \mathbb{R}^{N_k \times r_k}$. Each factor is approximated independently using the chosen real univariate approximation method \mathcal{F}_k .

Since $\mathcal{F}_1 \otimes \cdots \otimes \mathcal{F}_m$ is linear, we can also efficiently construct \hat{g} whenever \hat{G} is a linear combination of Tucker decompositions. This is called a *block term decomposition* [25]. We can also impose additional structure on C , such as a tree tensor network or *hierarchical Tucker decomposition* [34]. Linear combinations of such hierarchical Tucker decompositions are a special case of *structured block term decomposition* [28]. Without going into further details, we highlight that efficient construction of \hat{g} is possible for any structured block term decomposition.

Evidently, the curse of dimensionality is only truly circumvented if a data-sparse model can also be constructed from a *sparse* sample of the tensor G , i.e., from viewing only a few entries of G . In theory, this is possible for any polynomial-based decomposition model with a number of samples that equals the dimensionality of the model; see [16, 52] for precise statements. In practice, compressed sensing approximation schemes have been proposed for several tensor decomposition models; see, among others, [2, 3, 8, 35, 42, 48, 55, 56, 66].

The foregoing multivariate approximation scheme is naturally extended to approximate vector-valued g by applying it component-wise. We have chosen to present [Algorithm 4.1](#) with a basic orthogonal Tucker decomposition [26, 63] as data-sparse model, computed with the sequentially truncated higher-order singular value decomposition (ST-HOSVD) approximation algorithm [65] from the full tensor.

5. Numerical experiments. To illustrate [Algorithm 4.1](#) and to verify that the approximant it produces satisfies the error bounds predicted by [Theorem 3.1](#), we present some examples inspired by applications in linear algebra. All experiments were run on an HP EliteBook x360 830 G7 Notebook with 32 GiB memory and an Intel Core i7-10610U CPU using Julia 1.9.3 and `ManiFactor.jl` 0.1.0 on Ubuntu 22.04.3 LTS.

5.1. Implementation details and Julia package. [Algorithm 4.1](#) has been implemented in our Julia package, `ManiFactor.jl`, which is available online along with the experiments from this section [40]. Our package depends on the package `Manifolds.jl` by Axen, Baran, Bergmann, and Rzecki [7]. Many of the exponential and logarithmic maps for the manifolds in [Appendix A](#) are implemented there. Our package also depends on the package `ApproxFun.jl` by Olver and Townsend [47], which is a convenient interface to Chebyshev interpolation.

As [Lemma 4.1](#) implies that any suitable univariate scheme \mathcal{I} can be tensorized, `ManiFactor.jl` can use any such \mathcal{I} . Interesting alternatives to Chebyshev interpolation include Fourier-based schemes and rational approximation schemes.

Similarly, `ManiFactor.jl` can use any tensor decomposition. Specifically, it uses incomplete decompositions such as *TT-cross*, see Strössner, Sun, and Kressner [58]. The default is an ST-HOSVD from `TensorToolbox.jl` by Lana Periša [49].

5.2. An example from Krylov subspaces. In this example we approximate a map into the *Grassmannian manifold* $\text{Gr}(n, k)$ of k -dimensional linear subspaces of \mathbb{R}^n . See [Appendix A.2](#) for a discussion of its geometry. The example is inspired by Zimmermann’s discussion [69, section 4.5] of Grassmannians in the context of model order reduction, and Benner, Gugercin, and Willcox’s discussion [10] in the context of Krylov subspace methods.

Consider the heat equation [5, section 9.8] on a finite interval with endpoints held at a constant temperature 0:

$$(5.1) \quad \frac{\partial^2 u}{\partial x^2}(x, t) = a^2 \frac{\partial u}{\partial t}(x, t), \quad u(0, t) = 0, \quad u(\pi, t) = 0,$$

where a is a diffusion constant. For $t > 0$, u is determined by the *kernel*

$$(5.2) \quad K(x, x', t) = \frac{2}{\pi} \sum_{l=1}^{\infty} \sin(lx) \sin(lx') \exp(-ta^2 l^2).$$

That is,

$$(5.3) \quad u(x, t) = \int_0^{\pi} K(x, x', t) u(x', 0) dx'$$

is an explicit expression for u at time t in terms of u at time 0. By discretizing K along x and x' , we may approximate (5.3) as a matrix equation

$$(5.4) \quad A(t)y = b(t),$$

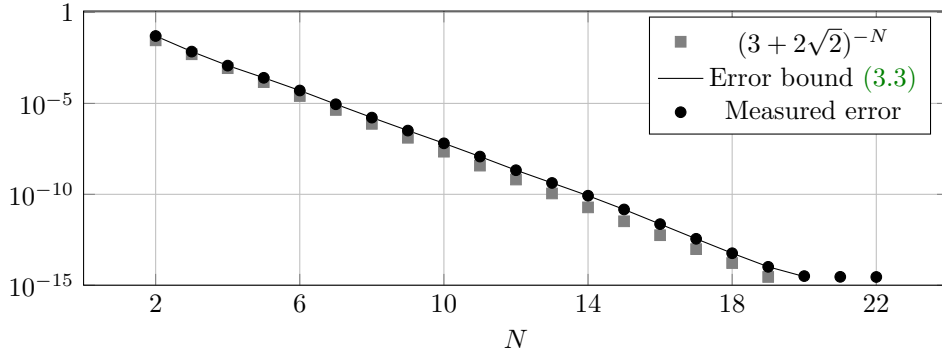


Fig. 5.1: Approximation error for the map (5.6) into the Grassmannian $\text{Gr}(n, k)$, compared against what is predicted by Theorem 3.1, for different numbers of Chebyshev nodes N .

where $A(t)$ is a $n \times n$ symmetric matrix with elements $A_{ij}(t) = \frac{\pi}{n-1} K(i \frac{\pi}{n-1}, j \frac{\pi}{n-1}, t)$, y is an n -vector with elements $y_i = u(i \frac{\pi}{n-1}, 0)$, and $b(t)$ is an n -vector with elements $b_i(t) = u(i \frac{\pi}{n-1}, t)$. Given this setup, consider the problem of finding a y that solves (5.4) for a given b .

Krylov subspace methods solve high-dimensional linear equations $Ay = b$ by looking for a solution in a *Krylov subspace*

$$(5.5) \quad \mathcal{K}_k(A, v) = \text{span} \{ v, Av, \dots, A^{k-1}v \}.$$

If we fix k and $v \in \mathbb{R}^n$, then

$$(5.6) \quad f(t) = \mathcal{K}_k(A(t), v)$$

is a map from \mathbb{R}^+ into $\text{Gr}(n, k)$.

Rather than compute the Krylov subspace from its definition for each t , we want to be able to quickly compute an approximate Krylov subspace. Because the dimension, $k(n-k)$, of $\text{Gr}(n, k)$, is much smaller for small k , than the dimension, n^2 , of the space that A lives in, such an approximation can be very profitable.

In this example, we approximate f on $R = [1, 2]$ with $a = 1/2$, $n = 100$, $k = 3$, and v sampled from a uniform distribution on $[-1, 1]^n$. These parameters are chosen such that, for $t \in R$, and for a normalized $b(t)$ in the image of $A(t)$, it is possible to find a y with forward error on the order of 10^{-3} using $\mathcal{K}_k(A(t), v)$. From there, it is straightforward to extend the Krylov subspace further by Arnoldi iteration.

We now proceed as in Algorithm 4.1. Choose p and let $g = \log_p \circ f$. Then consider the polynomial \hat{g} that interpolates g in $N + 1$ Chebyshev nodes on R . Finally, let $\hat{f} = \exp_p \circ \hat{g}$.

Since both f and the manifold logarithm are analytic, and because of Corollary 4.3, we expect the error $\|g - \hat{g}\|_p$ to decay at least exponentially in N . The actual expressions, however, seem too complicated to analyze analytically, but since f has a singularity at $t = 0$ (the series (5.2) fails to converge) we guess that this is the first singularity that you hit as you analytically extend g . In that case, $\|g - \hat{g}\|_p$ decays as $(3 + 2\sqrt{2})^{-N}$, and since $\text{Gr}(n, k)$ has nonnegative curvature, Theorem 3.1 implies $d(f, \hat{f}) \leq \|g - \hat{g}\|_p$.

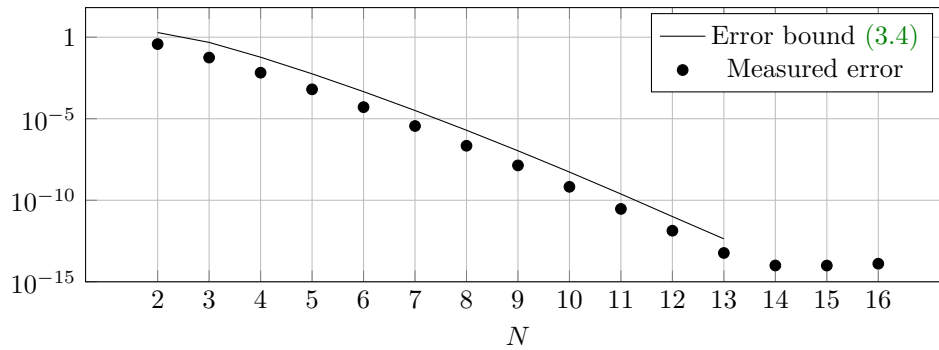


Fig. 5.2: Approximation error for the map (5.8) into the Segre manifold $\text{Seg}(\mathbb{R}^n \times \mathbb{R}^n)$, compared against what is predicted by Theorem 3.1, for different numbers of Chebyshev nodes N in each variable.

Indeed, the numerical experiment presented in Figure 5.1 supports this guess. In this experiment, we restrict f to a discrete subset $R' \subset R$ of 1000 points, sampled independently from a uniform distribution on R . We are thus able to use $\epsilon = \max_{x \in R'} \|g(x) - \hat{g}(x)\|_p$ in (3.3) to derive a bound for $d(f(x), \hat{f}(x))$. Figure 5.1 shows that this error bound is confirmed by the experiment. After $N = 20$, rounding causes the errors to plateau and the error bound stops being meaningful. The full code to produce Figure 5.1 is available in the `ManiFactor.jl` package [40, Example3.jl]

5.3. An example from dynamic low-rank approximation. Expanding on a synthetic example by Ceruti and Christian [17], we consider

$$(5.7) \quad A(x_1, x_2, x_3) = e^{x_1} e^{x_2 W_1} D (e^{x_3 W_2})^\top,$$

where D is an $n \times n$ diagonal matrix with diagonal entries $1, 2^{-1}, \dots, 2^{1-n}$, and W_1 and W_2 are skew-symmetric matrices, with entries sampled independently from a uniform distribution on $[-1, 1]$, and then normalized. Recall that when W is skew-symmetric, e^W is orthogonal. The best rank-1 approximation to A is

$$(5.8) \quad f(x) = e^{x_1} e^{x_2 W_1} e_1 (e^{x_3 W_2} e_1)^\top,$$

where e_1 is the column vector $(1, 0, \dots, 0)$. Thus f is a map from \mathbb{R}^3 into the Segre manifold of rank-1 matrices $\text{Seg}(\mathbb{R}^n \times \mathbb{R}^n)$. See Appendix A.3 for a discussion of its geometry. We approximate f on $R = [-1, 1]^3$ with $n = 100$.

Similarly to subsection 5.2, we proceed as Algorithm 4.1, while restricting to a discrete subset $R' \subset R$ of 1000 points sampled independently from a uniform distribution on R . Again, because of Corollary 4.3, we expect the error to decay exponentially in the number of Chebyshev nodes $N = N_1 = N_2 = N_3$. By (A.10), we have a lower bound $H = -e^2$ for the sectional curvature. Thus Theorem 3.1 implies that the approximation error is bounded by (3.4).

The numerical experiment presented in Figure 5.2 again confirms the error bound. After $N = 13$, rounding causes the errors to plateau and the error bound stops being meaningful. The full code to product Figure 5.2 is available in the `ManiFactor.jl` package [40, Example4.jl].

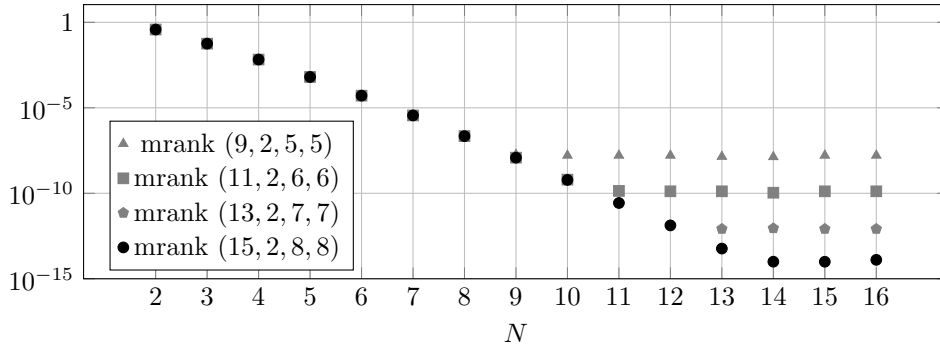


Fig. 5.3: Approximation error for a map into the Segre manifold $\text{Seg}(\mathbb{R}^n \times \mathbb{R}^n)$, with the tensor of samples is truncated at different multilinear ranks.

5.4. Effects of truncating the tensor decomposition. In subsection 4.2, we discussed how Algorithm 4.1 is implemented using a *sequentially truncated* HOSVD. We argued that working with sparse representations is key to circumventing the curse of dimensionality. We thus now illustrate how different levels of truncation affect the error. Consider again the example from subsection 5.3. Figure 5.3 shows the same numerical experiment, but with the decomposition of G truncated at different multilinear ranks (mrank).

Without truncation, G has $(2(n-1)+1)(N+1)^3$ entries since $\text{Seg}(\mathbb{R}^n \times \mathbb{R}^n)$ has dimension $2(n-1)+1$. Compare this to an ST-HOSVD \hat{G} of G with multilinear rank (r_0, r_1, r_2, r_3) , which only has $2(n-1)r_0 + (N+1)r_1 + (N+1)r_2 + (N+1)r_3 + r_0r_1r_2r_3$ entries. In Figure 5.3, we see that multilinear rank $(15, 2, 8, 8)$ is enough to reach machine precision at $N = 14$. In this case, G has 668 250 entries, while \hat{G} only has 5160 entries. The multilinear ranks are chosen automatically by `TensorToolbox.jl` to satisfy the error thresholds 10^{-6} , 10^{-8} , 10^{-10} , and 10^{-13} , respectively.

6. Conclusions. In conclusion, we find that the approximability of maps into a Riemannian manifold is related to the curvature of the manifold. Moreover, for many manifolds that are relevant for numerical analysis, especially matrix manifolds, explicit curvature bounds allow us to derive explicit error bounds.

From here, several areas of further research are visible. First, one could derive the geodesics and sectional curvature for more manifolds. For example spaces of tensors with fixed rank or multilinear rank. Second, one could develop more efficient and more optimal ways of choosing the point p from where the manifold is linearized. The current way, geodesic interpolation of sample evaluations, is a heuristic to estimate the Riemannian center of mass of those evaluations, which in turn is a heuristic to minimize σ in Theorem 3.1. Third, it could be possible to consider more than one tangent space. Given several approximations of f , based around several points, what is a good estimate of $f(x)$, and what are good ways of choosing such points?

Appendix A. Manifolds with lower bounded sectional curvature.

In this section, we list Riemannian manifolds with explicit lower bounds for their sectional curvature K and whose manifold exponential and logarithm are known. For these manifolds, Theorem 3.1 gives an explicit bound for the error on the manifold in terms of the error on the tangent space. While sectional curvature is always bounded

locally, for many manifolds that are relevant for applications we can find explicit expressions for those local bounds. In many cases, the sectional curvature is even bounded globally, so that we can choose the same H for every chart in [Theorem 3.1](#).

A.1. Lie groups. Given an inner product on its Lie algebra, one can extend it to a unique Riemannian metric on the Lie group by demanding invariance under left (or right) translation. Because of this invariance, the set of sectional curvatures at a point is independent of that point. Therefore, a lower bound for the sectional curvature at one point will be a global lower bound. There is an expression for the sectional curvature of a Lie group in terms of its Lie bracket [[21](#), Proposition 3.18 (3)]. We only note that, for matrix groups whose Lie algebra has the Euclidean inner product, it follows from this expression that¹

$$(A.1) \quad -\frac{11}{2} \leq K.$$

For example, $\mathrm{GL}(n)$ is the group of invertible $n \times n$ matrices. Its metric is induced by the inner product, $\langle u, v \rangle_A = \mathrm{tr}((A^{-1}u)^T A^{-1}v)$, where $u, v \in T_A \mathrm{GL}(n) = \mathbb{R}^{n \times n}$. Locally, all (finite-dimensional) Lie groups are Lie subgroups of some $\mathrm{GL}(n)$. Andruchow, Larotonda, Recht, and Varela [[4](#)] derive its geodesics.

The compact Lie groups and their products with vector spaces are precisely the Lie groups that admit a *bi-invariant* metric, i.e., a metric that is invariant under both left and right translation. This is also equivalent to the manifold exponential agreeing with the Lie group exponential. The sectional curvature is positive for such manifolds [[21](#), Corollary 3.19 and Proposition 3.34].

The classification of compact Lie groups is a classic result. The real compact Lie groups are [[6](#), Theorem 2.17]

- tori $S^1 \times \dots \times S^1$,
- orthogonal groups $\mathrm{O}(n)$ and special orthogonal groups $\mathrm{SO}(n)$,
- unitary groups $\mathrm{U}(n)$ and special unitary groups $\mathrm{SU}(n)$,
- spin groups $\mathrm{Spin}(n)$,
- symplectic groups $\mathrm{Sp}(n)$,
- compact exceptional Lie groups G_2 , F_4 , E_6 , and E_8 ,
- products, disjoint unions, and finite covers of the above.

A.2. Homogeneous spaces. A *Riemannian homogeneous space* is a Riemannian manifold equipped with some transitive action that the metric is invariant under. Similarly to Lie groups, the curvature is then the same at every point.

Any Riemannian homogeneous space X is of the form G/H where G is the Lie group that acts on X and H is a Lie subgroup. The *Stiefel manifold*

$$(A.2) \quad \mathrm{St}(n, k) = \mathrm{O}(n) / \mathrm{O}(n - k)$$

is the space of orthogonal $n \times k$ matrices. Zimmermann [[67](#)] considers efficient geodesic computations on the Stiefel manifold. It has nonnegative curvature.

The *Grassmannian manifold*

$$(A.3) \quad \mathrm{Gr}(n, k) = \mathrm{O}(n) / (\mathrm{O}(n - k) \times \mathrm{O}(k))$$

is the space of k -dimensional linear subspaces of \mathbb{R}^n . Bendokat, Zimmermann, and Absil [[9](#)] consider efficient geodesic computations on the Grassmannian manifold. It also has nonnegative curvature.

¹Using $\|[u, v]\| \leq \sqrt{2}\|u\|\|v\|$, which also implies $\|\mathrm{ad}_u\|_{\mathrm{op}} \leq \sqrt{2}\|u\|$.

For the Stiefel and Grassmannian manifolds, their metrics as Riemannian homogeneous spaces are called *canonical metrics* to distinguish them from their metrics as embedded submanifolds of $\mathbb{R}^{n \times n}$.

$\sigma_B: A \mapsto BAB^T$ defines a transitive action of $\mathrm{GL}(n)$ on the space \mathcal{P}_n of *symmetric positive definite $n \times n$ matrices*. The *affine invariant metric* on \mathcal{P}_n is thus derived from the quotient

$$(A.4) \quad \mathcal{P}_n = \mathrm{GL}(n) / \mathrm{O}(n).$$

Dolcetti and Pertici [29, Proposition 3.4] compute its geodesics, while Criscitiello and Boumal [24, Proposition I.1] show that its sectional curvature satisfies

$$(A.5) \quad -\frac{1}{2} \leq K \leq 0.$$

Similarly to \mathcal{P}_n , σ_B defines a transitive action of $\mathrm{GL}^+(n)$, the group of matrices with positive determinant, on the space $\mathrm{S}_+(n, k)$ of *rank- k positive semidefinite $n \times n$ matrices*. We have that

$$(A.6) \quad \mathrm{S}_+(n, k) = \mathrm{GL}^+(n) / \left(\left(\mathrm{SO}(k) \ltimes \mathbb{R}^{k \times (n-k)} \right) \times \mathrm{GL}^+(n-k) \right),$$

where \ltimes is the semidirect product. Vandereycken, Absil, and Vandewalle [64] use a right-invariant metric on $\mathrm{GL}^+(n)$ to derive geodesics on $\mathrm{S}_+(n, k)$.

We also mention another metric that can be put on the space of rank- k positive semidefinite matrices. Let $\mathbb{R}_*^{n \times k}$ be the space of full rank $n \times k$ matrices. Any rank- k positive semidefinite matrix can be written as YY^T , $Y \in \mathbb{R}_*^{n \times k}$. Such a representation is unique up to right multiplication by an orthogonal matrix. Hence, we define

$$(A.7) \quad \mathcal{S}_+(n, k) = \mathbb{R}_*^{n \times k} / \mathrm{O}(k),$$

where $\mathbb{R}_*^{n \times k}$ is equipped with the Euclidean metric. Although this manifold is not a Riemannian homogeneous space, a metric may still be induced by demanding that the quotient map is a Riemannian submersion. Massart and Absil [46] summarize its geometry. It has nonnegative curvature.

A.3. Segre manifold. The *Segre manifold*, $\mathrm{Seg}(\mathbb{R}^{N_1} \times \cdots \times \mathbb{R}^{N_m})$, is the space of rank-1 tensors in the product space $\mathbb{R}^{N_1} \otimes \cdots \otimes \mathbb{R}^{N_m}$ [37]. It is immersed by

$$(A.8) \quad \mathrm{Seg}: \mathbb{R}^+ \times S^{N_1-1} \times \cdots \times S^{N_m-1} \rightarrow \mathbb{R}^{N_1} \otimes \cdots \otimes \mathbb{R}^{N_m},$$

$$(A.9) \quad (\lambda, x_1, \dots, x_m) \mapsto \lambda x_1 \otimes \cdots \otimes x_m.$$

Swijsen, van der Veken, and Vannieuwenhoven [60] derives the exponential map for this manifold in the metric induced by the immersion. Moreover, Swijsen [59, Corollary 6.2.4] derive the manifold logarithm and shows that the sectional curvature satisfies

$$(A.10) \quad -\frac{1}{\lambda^2} \leq K \leq 0.$$

Note that in this case there is only a local lower bound, namely if the image of f fits in a chart with λ lower bounded by λ_* , then we may choose $H = -1/\lambda_*^2$.

REFERENCES

- [1] P.-A. ABSIL, R. MAHONY, AND R. SEPULCHRE, *Optimization Algorithms on Matrix Manifolds*, vol. 78, Princeton University Press, 12 2008.
- [2] E. ACAR, D. M. DUNLAVY, AND T. G. KOLDA, *A scalable optimization approach for fitting canonical tensor decompositions*, *Journal of Chemometrics*, 25 (2011), pp. 67–86.
- [3] E. ACAR, D. M. DUNLAVY, T. G. KOLDA, AND M. MØRUP, *Scalable tensor factorizations for incomplete data*, *Chemometrics and Intelligent Laboratory Systems*, 106 (2011), pp. 41–56.
- [4] E. ANDRUCHOW, G. LAROTONDA, L. RECHT, AND A. VARELA, *The left invariant metric in the general linear group*, *Journal of Geometry and Physics*, 86 (2014), pp. 241–257.
- [5] G. B. ARFKEN AND H.-J. WEBER, *Mathematical Methods for Physicists*, Elsevier Academic, 6 ed., 2005.
- [6] A. ARVANITOGEOGOS, *An Introduction to Lie Groups and the Geometry of Homogeneous Spaces*, American Mathematical Society, 2003.
- [7] S. D. AXEN, M. BARAN, R. BERGMANN, AND K. RZECKI, *Manifolds.jl: An extensible Julia framework for data analysis on manifolds*, 2023.
- [8] J. BALLANI, L. GRASEDYCK, AND M. KLUGE, *Black box approximation of tensors in hierarchical Tucker format*, *LAA*, 438 (2013), pp. 639–657.
- [9] T. BENDOKAT, R. ZIMMERMANN, AND P. A. ABSIL, *A Grassmann manifold handbook: Basic geometry and computational aspects*, 2023, 2011.13699. arxiv.org.
- [10] P. BENNER, S. GUGERCIN, AND K. WILLCOX, *A survey of projection-based model reduction methods for parametric dynamical systems*, *SIAM Review*, 57 (2015), pp. 483–531, <https://doi.org/10.1137/130932715>.
- [11] R. BERGMANN AND P.-Y. GOUSENBOURGER, *A variational model for data fitting on manifolds by minimizing the acceleration of a Bézier curve*, *Frontiers in Applied Mathematics and Statistics*, 4 (2018).
- [12] G. BEYLKIN AND M. J. MOHLENKAMP, *Numerical operator calculus in higher dimensions*, *Proceedings of the National Academy of Sciences of the United States of America*, 99 (2002), pp. 10246–10251.
- [13] ———, *Algorithms for numerical analysis in high dimensions*, *SIAM Journal on Scientific Computing*, 26 (2005), pp. 2133–2159.
- [14] D. BIGONI, A. P. ENGSIG-KARUP, AND Y. M. MARZOUK, *Spectral tensor-train decomposition*, *SIAM Journal on Scientific Computing*, 38 (2016), pp. A2405–A2439.
- [15] N. BOUMAL, *An Introduction to Optimization on Smooth Manifolds*, Cambridge University Press, Mar. 2023.
- [16] P. BREIDING, F. GESMUNDO, M. MICHALEK, AND N. VANNIEUWENHOVEN, *Algebraic compressed sensing*, *Applied and Computational Harmonic Analysis*, 65 (2023), pp. 374–406.
- [17] G. CERUTI AND L. CHRISTIAN, *An unconventional robust integrator for dynamical low-rank approximation*, *BIT Numerical Mathematics*, 62 (2022).
- [18] R. CHAKRABORTY AND B. C. VEMURI, *Recursive Fréchet mean computation on the Grassmannian and its applications to computer vision*, in *2015 IEEE International Conference on Computer Vision (ICCV)*, 2015, pp. 4229–4237.
- [19] ———, *Statistics on the Stiefel manifold: Theory and applications*, *The Annals of Statistics*, 47 (2019), pp. 415 – 438.
- [20] ———, *Efficient recursive estimation of the Riemannian barycenter on the hypersphere and the special orthogonal group with applications*, in *Riemannian Geometric Statistics in Medical Image Analysis*, X. Pennec, S. Sommer, and T. Fletcher, eds., Academic Press, 2020, pp. 273–297.
- [21] J. CHEEGER AND D. G. EBIN, *Comparison Theorems in Riemannian Geometry*, AMS Chelsea Publishing, 2008.
- [22] G. CHENG, J. HO, H. SALEHIAN, AND B. C. VEMURI, *Recursive Computation of the Fréchet Mean on Non-positively Curved Riemannian Manifolds with Applications*, Springer International Publishing, Cham, 2016, pp. 21–43.
- [23] O. CHRISTENSEN AND K. L. CHRISTENSEN, *Approximation Theory: from Taylor Polynomials to Wavelets*, Applied and Numerical Harmonic Analysis, Birkhäuser, 2004.
- [24] C. CRISCITIELLO AND N. BOUMAL, *An accelerated first-order method for non-convex optimization on manifolds*, 2021, 2008.02252. arxiv.org.
- [25] L. DE LATHAUWER, *Decompositions of a higher-order tensor in block terms—Part II: Definitions and uniqueness*, *SIAM Journal on Matrix Analysis and Applications*, 30 (2008), pp. 1033–1066.
- [26] L. DE LATHAUWER, B. DE MOOR, AND J. VANDEWALLE, *A multilinear singular value decomposition*, *SIAM Journal on Matrix Analysis and Applications*, 21 (2000), pp. 1253–1278.

- [27] T. DE WEER, N. VANNIEUWENHOVEN, N. LAMMENS, AND K. MEERBERGEN, *The parametrized superelement approach for lattice joint modelling and simulation*, Computational Mechanics, 70 (2022), pp. 451–475.
- [28] N. DEWAELE, P. BREIDING, AND N. VANNIEUWENHOVEN, *The condition number of many tensor decompositions is invariant under tucker compression*, Numerical Algorithms, 94 (2023), pp. 1003–1029.
- [29] A. DOLCETTI AND D. PERTICI, *Differential properties of spaces of symmetric real matrices*, 2018, 1807.01113. arxiv.org.
- [30] S. DOLGOV, D. KRESSNER, AND C. STRÖSSNER, *Functional tucker approximation using chebyshev interpolation*, SIAM Journal on Scientific Computing, 43 (2021), pp. A2190–A2210, <https://doi.org/10.1137/20M1356944>.
- [31] K. GLAU, D. KRESSNER, AND F. STATTI, *Low-rank tensor approximation for Chebyshev interpolation in parametric option pricing*, SIAM Journal on Financial Mathematics, 11 (2020), pp. 897–927.
- [32] A. GORODETSKY, S. KARAMAN, AND Y. MARZOUK, *A continuous analogue of the tensor-train decomposition*, Computer Methods in Applied Mechanics and Engineering, 347 (2019), pp. 59–84.
- [33] P.-Y. GOUSENBOURGER, E. MASSART, AND P.-A. ABSIL, *Data fitting on manifolds with composite Bézier-like curves and blended cubic splines*, Journal of Mathematical Imaging and Vision, 61 (2019), pp. 645–671.
- [34] L. GRASEDYCK, *Hierarchical singular value decomposition of tensors*, SIAM Journal on Matrix Analysis and Applications, 31 (2010), pp. 2029–2054.
- [35] L. GRASEDYCK, M. KLUGE, AND S. KRÄMER, *Variants of alternating least squares tensor completion in the tensor train format*, SIAM Journal on Scientific Computing, 37 (2015), pp. A2424–A2450.
- [36] W. H. GREUB, *Multilinear algebra*, Die Grundlehren der mathematischen Wissenschaften: 136, Springer, 2 ed., 1978.
- [37] J. HARRIS, *Algebraic Geometry, A First Course*, vol. 133 of Graduate Text in Mathematics, Springer-Verlag, 1992.
- [38] B. HASHEMI AND Y. NAKATSUKASA, *On the spectral problem for trivariate functions*, BIT Numerical Mathematics, 58 (2018), pp. 981–1008.
- [39] B. HASHEMI AND L. N. TREFETHEN, *Chebfun in three dimensions*, SIAM Journal on Scientific Computing, 39 (2017), pp. C341–C363.
- [40] S. JACOBSSON, *ManiFactor.jl: Approximating maps into manifolds*. <https://gitlab.kuleuven.be/numa/software/ManiFactor>, 2024.
- [41] H. KARCHER, *Riemannian center of mass and mollifier smoothing*, Communications on Pure and Applied Mathematics, 30 (1977), pp. 509–541.
- [42] D. KRESSNER, M. STEINLECHNER, AND B. VANDEREYCKEN, *Low-rank tensor completion by Riemannian optimization*, BIT Numerical Mathematics, 54 (2014), pp. 447–468.
- [43] J. M. LEE, *Introduction to Smooth Manifolds*, Graduate texts in mathematics: 218, Springer, 2013.
- [44] ———, *Introduction to Riemannian Manifolds.*, Graduate texts in mathematics: 176, Springer, 2018.
- [45] J. MASON, *Near-best multivariate approximation by Fourier series, Chebyshev series and Chebyshev interpolation*, Journal of Approximation Theory, 28 (1980), pp. 349–358.
- [46] E. MASSART AND P.-A. ABSIL, *Quotient geometry with simple geodesics for the manifold of fixed-rank positive-semidefinite matrices*, SIAM Journal on Matrix Analysis and Applications, 41 (2020), pp. 171–198, <https://doi.org/10.1137/18M1231389>.
- [47] S. OLVER AND A. TOWNSEND, *A practical framework for infinite-dimensional linear algebra*, in Proceedings of the 1st Workshop for High Performance Technical Computing in Dynamic Languages – HPTCDL ‘14, IEEE, 2014.
- [48] I. V. OSELEDETS AND E. TYRTYSHNIKOV, *TT-cross approximation for multidimensional arrays*, Linear Algebra and its Applications, 432 (2010), pp. 70–88.
- [49] L. PERIŠA, *TensorToolbox.jl: Julia package for tensors*. <https://github.com/lanaperisa/TensorToolbox.jl>, 2023.
- [50] M. REID AND B. SZENDROI, *Geometry and Topology*, Cambridge University Press, 2005.
- [51] J. R. RICE, *A theory of condition*, SIAM Journal on Numerical Analysis, 3 (1966), pp. 287–310, <https://doi.org/10.1137/0703023>.
- [52] Y. RONG, Y. WANG, AND Z. XU, *Almost everywhere injectivity conditions for the matrix recovery problem*, Applied and Computational Harmonic Analysis, 50 (2021), pp. 386–400.
- [53] M. H. SCHULTZ, *L^∞ -multivariate approximation theory*, SIAM Journal on Numerical Analysis, 6 (1969), pp. 161–183.

- [54] T. SHI AND A. TOWNSEND, *On the compressibility of tensors*, SIAM Journal on Matrix Analysis and Applications, 42 (2021), pp. 275–298.
- [55] M. SIGNORETTO, Q. TRAN DINH, L. DE LATHAUWER, AND J. A. K. SUYKENS, *Learning with tensors: a framework based on convex optimization and spectral regularization*, Machine Learning, 94 (2013), pp. 303–351.
- [56] M. STEINLECHNER, *Riemannian optimization for high-dimensional tensor completion*, SIAM Journal on Scientific Computing, 38 (2016), pp. S461–S484.
- [57] C. STRÖSSNER AND D. KRESSNER, *Low-rank tensor approximations for solving multimarginal optimal transport problems*, SIAM Journal on Imaging Sciences, 16 (2023), pp. 169–191, <https://doi.org/10.1137/22M1478355>.
- [58] C. STRÖSSNER, B. SUN, AND D. KRESSNER, *Approximation in the extended functional tensor train format*, 2022, 2211.11338. arxiv.org.
- [59] L. SWIJSEN, *Tensor decompositions and Riemannian optimization*, PhD thesis, KU Leuven, 2022.
- [60] L. SWIJSEN, J. VAN DER VEKEN, AND N. VANNIEUWENHOVEN, *Tensor completion using geodesics on Segre manifolds*, Numerical Linear Algebra with Applications, 29 (2022).
- [61] V. TEMLYAKOV, *Multivariate Approximation*, Cambridge Monographs on Applied and Computational Mathematics, Cambridge University Press, 2018.
- [62] L. N. TREFETHEN, *Approximation Theory and Approximation Practice, Extended Edition*, Society for Industrial and Applied Mathematics, Philadelphia, PA, 2019, <https://epubs.siam.org/doi/pdf/10.1137/1.9781611975949>.
- [63] L. R. TUCKER, *Some mathematical notes on three-mode factor analysis*, Psychometrika, 31 (1966), pp. 279–311.
- [64] B. VANDEREYCKEN, P.-A. ABSIL, AND S. VANDEWALLE, *A Riemannian geometry with complete geodesics for the set of positive semidefinite matrices of fixed rank*, IMA Journal of Numerical Analysis, 33 (2012), pp. 481–514, <https://academic.oup.com/imajna/article-pdf/33/2/481/1845277/drs006.pdf>.
- [65] N. VANNIEUWENHOVEN, R. VANDEBRIL, AND K. MEERBERGEN, *A new truncation strategy for the higher-order singular value decomposition*, SIAM Journal on Scientific Computing, 34 (2012), pp. A1027–A1052, <https://doi.org/10.1137/110836067>.
- [66] N. VERVLLET, O. DEBALS, L. SORBER, AND L. DE LATHAUWER, *Breaking the curse of dimensionality using decompositions of incomplete tensors: Tensor-based scientific computing in big data analysis*, IEEE Signal Processing Magazine, 31 (2014), pp. 71–79.
- [67] R. ZIMMERMANN, *A matrix-algebraic algorithm for the Riemannian logarithm on the Stiefel manifold under the canonical metric*, SIAM Journal on Matrix Analysis and Applications, 38 (2017), pp. 322–342, <https://doi.org/10.1137/16M1074485>.
- [68] ———, *Hermite interpolation and data processing errors on Riemannian matrix manifolds*, SIAM Journal on Scientific Computing, 42 (2020), pp. A2593–A2619, <https://doi.org/10.1137/19M1282878>.
- [69] ———, *Manifold interpolation and model reduction*, 2022, 1902.06502.
- [70] R. ZIMMERMANN AND R. BERGMANN, *Multivariate Hermite interpolation of manifold-valued data*, 2022, 2212.07281. arxiv.org.